PCCP

ROYAL SOCIETY OF CHEMISTRY

PAPER

View Article Online
View Journal | View Issue

Cite this: *Phys. Chem. Chem. Phys.*, 2022, **24**, 7264

Disentangling enantiosensitivity from dichroism using bichromatic fields

Andres F. Ordonez [ab] and Olga Smirnova [ac]

We discuss how tensorial observables, available in photoelectron angular distributions resulting from interaction between isotropic chiral samples and cross polarized ω–2ω bichromatic fields, allow for chiral discrimination without chiral light and within the electric-dipole approximation. We extend the concept of chiral setup [A. F. Ordonez and O. Smirnova, *Phys. Rev. A*, 2018, **98**, 063428], which explains how chiral discrimination can be achieved in the absence of chiral light, to the case of tensorial observables. We derive selection rules for the enantiosensitivity and dichroism of the $b_{l,m}$ coefficients describing the photoelectron angular distribution valid for both weak and strong fields and for arbitrary ω–2ω relative phase. Explicit expressions for simple perturbative cases are given. We find that, besides the known dichroic non-enantiosensitive [R. E. Goetz, C. P. Koch and L. Greenman, *J. Chem. Phys.*, 2019, **151**, 074106], and dichroic-and-enantiosensitive $b_{l,m}$ coefficients found recently [P. V. Demekhin, *Phys. Rev. A*, 2019, **99**, 063406], there are also enantiosensitive non-dichroic $b_{l,m}$ coefficients. These reveal the molecular enantiomer independently of the relative phase between the two colors and are therefore observable even in the absence of stabilization of the ω–2ω relative phase.

Received 21st December 2021,
Accepted 17th February 2022

DOI: 10.1039/d1cp05833a

rsc.li/pccp

1 Introduction

More than two centuries after the pioneering observations of Biot and Arago,[1] the interaction between light and chiral matter[2] remains a very active field of research.[3–7] This research effort is fueled not only by the interest in finding new ways of manipulating light and matter but also by the homochirality of life. While the molecule–molecule interactions that take place in biological systems are often strongly enantiosensitive,[8] the enantiosensitive response in "traditional" light–matter interactions is usually very weak. This weakness, which limits the potential of light-based applications, is prevalent in situations where the electric–dipole approximation is well justified but the chiral effects appear as small corrections such as the magnetic-dipole interaction.[9] Besides ingenious methods to cope with such situations,[10–12] weakly enantiosensitive responses can be avoided from the outset by relying on chiral effects occurring within the electric–dipole approximation.[13,14]

Among the chiral electric–dipole effects, photoelectron circular dichroism (PECD)[15–19] is very well established and has been shown to consistently yield strongly enantiosensitive signals across many molecular species[20] and different photoionization regimes.[21,22] In PECD, isotropically oriented chiral molecules are photoionized using circularly polarized light and the photoelectron angular distribution displays a so-called forward–backward asymmetry (asymmetry with respect to the polarization plane). This asymmetry is both enantiosensitive (opposite for opposite enantiomers) and dichroic (opposite for opposite polarizations), and results from the lack of mirror symmetry of the chiral molecules (and thus of the light-matter system) with respect to the plane of polarization. For an isotropically oriented achiral molecule and within the electric-dipole approximation (*i.e.* ignoring light-propagation effects), the light-matter system is mirror-symmetric with respect to the polarization plane and therefore forward–backward asymmetric observables resulting from a single-molecule response are symmetry-forbidden. For a randomly oriented chiral molecule the mirror symmetry of the light-matter system is absent and there are usually no further symmetries preventing the emergence of forward–backward asymmetric observables. In the one-photon case, the forward–backward asymmetry results from the non-zero molecular rotational invariant describing the average circular polarization of the photoionization-dipole vector field.[23]

Very recently, the response of chiral molecules to more elaborate field polarizations has been investigated in the multi-photon and strong-field regimes.[24–26] In these works, encompassing theory[24–26] and experiment,[26] a bichromatic field with frequencies ω and 2ω linearly polarized perpendicular to each other yields a new type of enantiosensitive and dichroic

[a] *Max-Born-Institut, 12489 Berlin, Germany*
[b] *ICFO-Institut de Ciencies Fotoniques, The Barcelona Institute of Science and Technology, 08860 Barcelona, Spain. E-mail: andres.ordonez@icfo.eu*
[c] *Technische Universität Berlin, 10623, Berlin, Germany. E-mail: olga.smirnova@mbi-berlin.de*

asymmetry in the photoelectron angular distribution. The Lissajous figure of this bichromatic field has an eight-like shape for particular phase relations between the two colors, and therefore ''rotates'' in opposite directions in the first and second halves of its cycle, with the direction of rotation of the field locked to the sign of its ω component. For example, the rotation is clockwise when the ω component is positive and counterclockwise when the ω component is negative. The observed asymmetry in the photoelectron angular distribution corresponds to a correlation between the so-called forward–backward direction and the up-down direction determined by the ω field (see Fig. 1 in ref. 24). So far, this asymmetry has been analyzed on the basis of a subcycle PECD-like picture where electrons detected in the upper hemisphere have an *e.g.* positive forward–backward asymmetry because they were produced by a field rotating *e.g.* clockwise, while the electrons detected in the lower hemisphere have a negative forward–backward asymmetry because they were produced by a field rotating counterclockwise.[24,26] Extensions of this reasoning to account for non-zero asymmetries for other relative phases between the ω and 2ω components have been considered in ref. 25 and 26.

Here we approach the description of the photoelectron angular distribution taking explicitly into account its tensorial character, the role of tensorial detectors in forming the chiral setup required to distinguish between opposite enantiomers, and the symmetry of the light-matter system. In Section 2 we discuss general considerations regarding how to distinguish between opposite enantiomers in isotropic samples without relying on the chirality of a light field. In Section 3 we discuss how tensorial observables can be used for the construction of chiral setups. In Section 4 we consider the interaction of an ω–2ω cross polarized field with isotropic molecular samples and derive selection rules for multipolar observables. Then we consider the perturbative description of photoionization and exploit the technique presented in ref. 23 to obtain explicit formulas for some representative $\tilde{b}_{l,m}$ coefficients of the photoelectron angular distribution displaying different combinations of dichroism and enantiosensitivity. Finally, we list our conclusions in Section 5. Analogous results but for the case of charge multipoles induced *via* excitation of bound states are presented in ref. 27.

2 Chiral probes

Distinguishing between the left version (L) and the right version (R) of a chiral object invariably requires interaction with another chiral object (say R′). The difference between the interactions L + R′ and R + R′ is the essence of any enantiosensitive phenomenon. Here we are interested in phenomena where light is used to distinguish between opposite enantiomers of isotropically oriented chiral molecules. In the simplest case, one lets circularly polarized light of a given handedness interact with a chiral sample and measures a scalar, namely the amount of light that is absorbed. In this situation, known as circular dichroism (CD), the chiral probe is the circularly polarized light and its handedness (a pseudoscalar) is given by its helicity, *i.e.* the projection of the photon spin (the rotation direction of the light at a given point in space, a pseudovector) on the propagation direction of the light (a vector). Another canonical example is optical activity, where one passes linearly polarized light through a chiral sample and measures the rotation of the polarization plane. In this case one measures an angle (a pseudovector). To measure it one must define a positive and a negative direction in the laboratory frame. Although such definition is just as arbitrary as defining what is left and what is right, it is a fundamental step in the measurement process. Once it has been defined, the handedness of the probe is given by the projection of the positive unit angle pseudovector on the propagation direction of the light (see Fig. 8 in ref. 14). That is, the chiral probe in this case is the chiral setup formed by the (achiral) light and the (achiral) detector (which encodes the definition of positive and negative rotations) together. This shows how a chiral setup may probe the handedness of a molecule in the absence of chiral light.

Circular dichroism and optical activity have in common that the handedness of the chiral probe relies on the propagation direction of the light. Since that propagation direction is immaterial within the electric-dipole approximation, unless one considers corrections to the electric-dipole approximation the probe ceases to be chiral and both effects vanish. To the extent that such corrections are typically small at the single molecule level, these effects are also correspondingly small. In order to obtain bigger enantiosensitive signals at the single-molecule level, a probe which is chiral within the electric-dipole approximation is required. Furthermore, if the result of the measurement is a scalar (like in circular dichroism), the light itself must be chiral. The concept of light which is chiral within the electric-dipole approximation, *i.e.* locally-chiral light, has been recently developed in ref. 6. If the result of the measurement is a polar vector, such as a net photoelectron current along a Cartesian axis, then the detector required to measure the vector must define (again, in an arbitrary fashion) a positive and a negative direction. In addition, if the polarization of the light allows the definition of a pseudovector, as is the case for example for circularly polarized light, where the pseudovector indicates the photon's spin, then one can define a chiral setup with its handedness given by the projection of the light pseudovector on the positive direction defined by the detector. This type of chiral setup is common to a series of recently discovered phenomena that range from rotational dynamics[28–30] to photoionization,[15–18] and it was recently discussed in ref. 13. In what follows we will extend the concept of chiral setups, to include those that rely on tensors of rank 2 (relevant for the results in ref. 24–26) and higher.

3 Tensor observables and chiral setups

Second and higher-rank tensors emerge naturally for observables which depend on a vector. Charge densities and photoelectron angular distributions (PADs) offer exactly such kind of

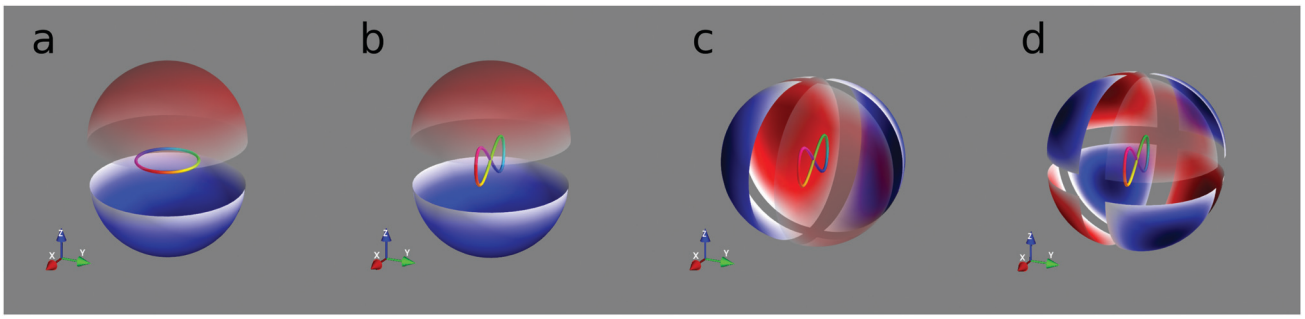

Fig. 1 Chiral (a, c and d) and achiral (b) setups consisting of a Lissajous figure and detectors. Counts on red/blue detectors are added/subtracted. The color of the Lissajous figure indicates the phase of the oscillation. (a) A field circularly polarized in the xy plane and a detector for $\tilde{b}_{1,0}$. (b), (c), and (d) A cross-polarized ω–2ω field in the xz plane and a detector for $\tilde{b}_{1,0}$, $\tilde{b}_{2,-2}$ and $\tilde{b}_{3,-2}$, respectively.

observable and, as any other function which depends on a vector, they can be expanded as

$$W(\vec{k}) = \sum_{l,m} \tilde{b}_{l,m}(k)\,\tilde{Y}_l^m(\hat{k}), \tag{1}$$

where $\vec{k}$ is the photoelectron momentum and we have chosen to do the expansion in terms of real spherical harmonics $\tilde{Y}_l^m$. In the case of a charge distribution we replace the photoelectron momentum $\vec{k}$ by the position $\vec{r}$ and $\tilde{b}_{l,m}$ could be a time dependent quantity.[27] The $\tilde{b}_{l,m}$ coefficients not only encode all the information contained in $W(\vec{k})$ but are also examples of tensors of rank l (see *e.g.* Section 4.10 in ref. 31).

In principle, the measurement of a particular $\tilde{b}_{l,m}$ coefficient can be performed directly by using a detector with a structure that reflects the corresponding $\tilde{Y}_l^m$. For example, a detector for $\tilde{b}_{0,0}$ would simply sum the counts in all directions. A detector for $\tilde{b}_{1,0}$ would have two plates arranged as in Fig. 1a and b, so that it would add all the counts on one of them (red) and subtract all the counts on the other (blue). The choice of which plate adds and which plate subtracts is what physically defines the $\hat{z}$ direction of the laboratory frame. A detector for $\tilde{b}_{2,-2}$ would have four plates arranged as in Fig. 1c, with a pair of opposite plates adding counts and the other pair subtracting counts. In this case, the detector defines the directions that correspond to a positive correlation between x and y, and those that correspond to a negative correlation between x and y. Analogously, a detector for $\tilde{b}_{3,-2}$ has eight plates arranged as in Fig. 1d, and distinguishes positive from negative correlations of x, y, and z.

The combination of a $\tilde{b}_{l,m}$-specific detector and the Lissajous figure of the electric field can make up a chiral setup as shown in Fig. 1a, c and d. These setups are non-superimposable on their mirror images. This is particularly simple to see in Fig. 1a, c and d for reflections with respect to the polarization plane, which do not change the Lissajous figure but do swap blue and red plates. The chirality of these setups allows them to distinguish between opposite enantiomers of a chiral molecule. This is in contrast with the setup in Fig. 1b, which is symmetric with respect to reflection in the polarization plane and thus is not chiral and cannot distinguish between opposite enantiomers of a chiral molecule.

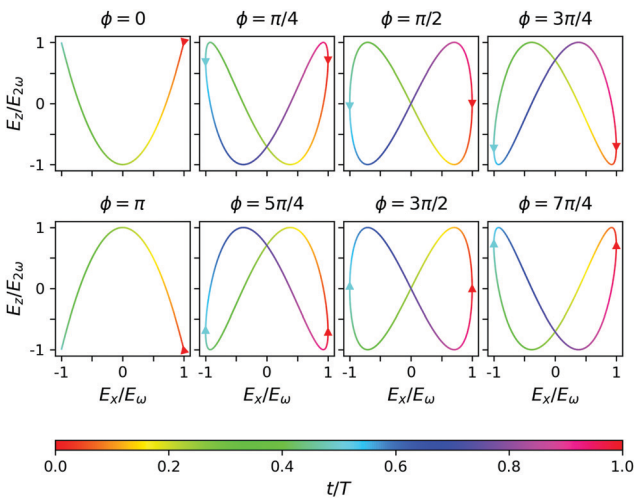

Fig. 2 Lissajous curves of the field (2) for different values of ϕ. The position of the red arrow indicates t = 0.

Of course, a chiral setup is only relevant if the light-matter system is indeed asymmetric enough that it can yield a corresponding non-zero $\tilde{b}_{l,m}$. In other words, the concept of a chiral setup answers the question of how we can distinguish opposite enantiomers without relying on the chirality of light, but it is the lack of symmetry of the light-matter system itself the deciding factor which determines the emergence of an enantiosensitive observable in the first place (see *e.g.* Fig. 2 in ref. 13). We now turn to the analysis of a specific family of Lissajous figures to illustrate this in detail.

4 ω–2ω cross polarized field

Consider a two-color field of the form

$$\vec{E}(t) = E_\omega \cos(\omega t)\hat{x} + E_{2\omega}\cos(2\omega t + \phi)\hat{z} \tag{2}$$

This field is illustrated in Fig. 2 for different phases† ϕ. If we denote rotations by π around the z axis by $\hat{R}_z^\pi$ and time shifts of

† Our choice of axes, which differs from ref. 22–24, simplifies Table 1. Our choice of phase coincides with that in ref. 24 and differs from the one in ref. 22 and 23. Note that some of the plots of Fig. 2(a) in ref. 24 are labeled with the wrong phase.

Table 1 Conditions imposed by symmetry on the $\tilde{b}_{l,m}$ coefficients describing the photoelectron angular distribution (1) resulting from the interaction between an isotropic molecular sample and the field (2)

$\tilde{b}_{l,m}$	(l,m) condition
Symmetry-allowed at $2n\omega$	Even m
Symmetry-allowed at $(2n+1)\omega$	Odd m
Enantiosensitive	$m < 0$
Dichroic	[(Odd $l-m$) and ($m \geq 0$)] or (even $l-m$) and ($m < 0$)

π/ω by $T_{\pi/\omega}$, then the joint system (field and isotropic chiral molecules) is invariant with respect to $\hat{R}_z^{\pi}\hat{T}_{\pi/\omega}$. Clearly, the resulting observables must also be invariant with respect to $\hat{R}_z^{\pi}\hat{T}_{\pi/\omega}$. That is, the symmetry-allowed $\tilde{b}_{l,m}$ coefficients must satisfy $\hat{R}_z^{\pi}\hat{T}_{\pi/\omega}\tilde{b}_{l,m}\tilde{Y}_l^m = \tilde{b}_{l,m}\tilde{Y}_l^m$. This corresponds to two scenarios: either $\hat{R}_z^{\pi}\tilde{Y}_l^m = \tilde{Y}_l^m$ and $\tilde{b}_{l,m}$ contains only frequencies $2n\omega$, or $\hat{R}_z^{\pi}\tilde{Y}_l^m = -\tilde{Y}_l^m$ and $\tilde{b}_{l,m}$ contains only frequencies $(2n+1)\omega$, where $n = 0, 1, 2, \ldots$. Furthermore, since a reflection $\hat{\sigma}_y$ with respect to the $y = 0$ plane swaps the enantiomers while leaving the field invariant, an enantiosensitive $\tilde{b}_{l,m}$ is associated to a $\tilde{Y}_l^m$ satisfying $\hat{\sigma}_y\tilde{Y}_l^m = -\tilde{Y}_l^m$. And, since a rotation $\hat{R}_x^{\pi}$ of π around the x axis changes the phase ϕ in the field by π while leaving the molecules invariant, a dichroic‡ $\tilde{b}_{l,m}$ is associated to a $\tilde{Y}_l^m$ satisfying $\hat{R}_x^{\pi}\tilde{Y}_l^m = -\tilde{Y}_l^m$. These properties, which are valid independently of the ionization regime, are summarized in Tables 1 and 2.

Evidently, the values of l and m that determine whether a given $\tilde{b}_{l,m}$ is symmetry-allowed and whether it is enantiosensitive and/or dichroic depends on how the field is oriented with respect to the axes. The choice made here [eqn (2)] yields the rather simple conditions in Tables 1 and 2. Conditions corresponding to other choices are given in Appendix A for the sake of comparison with ref. 24–26.

Tables 1 and 2 reveal two important features. First, the spatial structure of the response depends on whether it oscillates with a frequency which is an even (including zero) or an odd multiple of the fundamental frequency (see also ref. 32). Second, in contrast to a circularly polarized field where dichroism goes hand in hand with enantiosensitivity, the symmetry of the field (2) leads to four types of signals:

(i) Non-dichroic and non-enantiosensitive.
(ii) Dichroic and enantiosensitive.
(iii) Dichroic and non-enantiosensitive.
(iv) Enantiosensitive and non-dichroic.

Type (i) and type (ii) signals are well known from traditional CD and PECD. Type (iii) signals are well known in atoms subject to light fields whose Lissajous figure is not symmetric under spatial inversion.[33] They have also been recently calculated for the case of randomly oriented chiral molecules[34] for parallel polarizations of ω and 2ω. Here, type (iii) signals are due to the asymmetry of the field (2) along the z direction (see Fig. 2). Type (iv) signals are more exotic but apparently they can also occur in the context of magnetic effects beyond the electric-dipole approximation,[35,36] where to the best of our knowledge they remain to be confirmed by experiment. As we will show next, photoionization may prove to be a better candidate for experimentally measuring type (iv) signals.

‡ Here we use the word dichroic in analogy to how it is used in the circularly polarized case in PECD, where a change of π in the phase between the two perpendicular components of the field leads to a change of sign of $b_{1,0}$.

4.1 Photoionization

The photoelectron angular distribution accumulated over many cycles of the field (2) corresponds to a signal with zero frequency and must satisfy the conditions given in Table 1 for frequencies $2n\omega$. For convenience, we list the properties of the symmetry-allowed $\tilde{b}_{l,m}$ coefficients for l up to four in Table 3. From this table we can see that *e.g.* $\tilde{b}_{1,0}$ is dichroic but not enantiosensitive, $\tilde{b}_{2,-2}$ is enantiosensitive and dichroic, and $\tilde{b}_{3,-2}$ is enantiosensitive but not dichroic. Since $\tilde{Y}_1^0(\hat{k}) \propto k_z$, $\tilde{Y}_2^{-2}(\hat{k}) \propto k_xk_y$, and $\tilde{Y}_3^{-2}(\hat{k}) \propto k_xk_yk_z$, then $\tilde{b}_{1,0}$ is associated to asymmetry along the direction of the 2ω field ($\hat{z}$), $\tilde{b}_{2,-2}$ is associated to correlations between the direction of the ω field ($\hat{x}$) and the direction perpendicular to the polarization plane ($\hat{y}$), and $\tilde{b}_{3,-2}$ is associated to correlations of the three directions corresponding to the ω field ($\hat{x}$), the 2ω field ($\hat{z}$), and the perpendicular to the polarization plane ($\hat{y}$).

In ref. 23 we showed that, in general, a $\tilde{b}_{l,m}$ coefficient is enantiosensitive if and only if it results from interference between pathways with N_1 and N_2 photons, respectively, and $l + N_1 + N_2$ is odd; or if it results from a direct pathway and l is odd. These conditions together with Table 2 tell us that a dichroic non-enantiosensitive $\tilde{b}_{l,m}$ (with odd l) can only occur as the result of interference between pathways involving an even and an odd number of photons, respectively (so that $N_1 + N_2$ is odd and $l + N_1 + N_2$ is even). For example, $\tilde{b}_{1,0}$ contributes to the photoelectron peak where absorption of two ω photons interferes with absorption of one 2ω photon (see Fig. 3a). The same condition (odd $N_1 + N_2$) applies for a dichroic and enantiosensitive $\tilde{b}_{l,m}$ (even l) such as $\tilde{b}_{2,-2}$. In contrast, an enantiosensitive non-dichroic $\tilde{b}_{l,m}$ (odd l) can occur as the result of either a direct pathway involving at least one ω photon and one 2ω photon, or as the result of interference between two pathways both with an even or both with an odd number of photons (even $N_1 + N_2$). For example, $\tilde{b}_{3,-2}$ contributes to the photoelectron peak corresponding to absorption of one ω photon followed by absorption of one 2ω photon (see Fig. 3b) and *vice versa*, or as the result of interference between absorption of two 2ω photons and four ω photons.

As an example, let us calculate explicit expressions for $\tilde{b}_{1,0}$, $\tilde{b}_{2,-2}$, and $\tilde{b}_{3,-2}$. For the process depicted in Fig. 3a, the interference between the two pathways gives rise to a non-zero orientation-averaged $\tilde{b}_{1,0}$ given by (see Appendix B)

$$\tilde{b}_{1,0}(k) = A^{(1)*}A^{(2)}g_{1,0}f_{1,0} + \text{c.c.}, \quad (3)$$

where $A^{(1)}$ and $A^{(2)}$ are complex-valued constants depending on detunings and pulse envelopes, c.c. denotes the complex conjugate, $g_{1,0}$ is a (complex-valued) molecular rotational invariant, and $f_{1,0}$ is a setup (*i.e.* field + detector) rotational invariant. $g_{1,0}$ is a scalar§ (in contrast to a pseudoscalar) and therefore $\tilde{b}_{1,0}$ is

§ Explicit expressions for the molecular rotational invariants $g_{1,-1}$, $g_{2,-2}$, and $g_{3,-2}$ are given in Appendices B–D.

Table 2 (l,m) conditions derived from Table 1 for non-vanishing enantiosensitive and/or dichroic $\tilde{b}_{l,m}$ coefficients

Symmetry-allowed $\tilde{b}_{l,m}$	(l,m) condition at $2n\omega$	(l,m) condition at $(2n+1)\omega$
Enantiosensitive and dichroic	(Even l) and (even $m < 0$)	(Odd l) and (odd $m < 0$)
Enantiosensitive non-dichroic	(Odd l) and (even $m < 0$)	(Even l) and (odd $m < 0$)
Dichroic non-enantiosensitive	(Odd l) and (even $m > 0$)	(Even l) and (odd $m > 0$)

Table 3 Dichroism and enantiosensitivity of symmetry-allowed $\tilde{b}_{l,m}$ coefficients describing the photoelectron angular distribution (1) resulting from interaction of an isotropic molecular sample and the field (2) for l up to 4. N = No and Y = Yes

Symmetry-allowed	$\tilde{b}_{0,0}$	$\tilde{b}_{1,0}$	$\tilde{b}_{2,-2}$	$\tilde{b}_{2,0}$	$\tilde{b}_{2,2}$	$\tilde{b}_{3,-2}$	$\tilde{b}_{3,0}$	$\tilde{b}_{3,2}$	$\tilde{b}_{4,-4}$	$\tilde{b}_{4,-2}$	$\tilde{b}_{4,0}$	$\tilde{b}_{4,2}$	$\tilde{b}_{4,4}$
Enantiosensitive	N	N	Y	N	N	Y	N	N	Y	Y	N	N	N
Dichroic	N	Y	Y	N	N	N	Y	Y	Y	Y	N	N	N

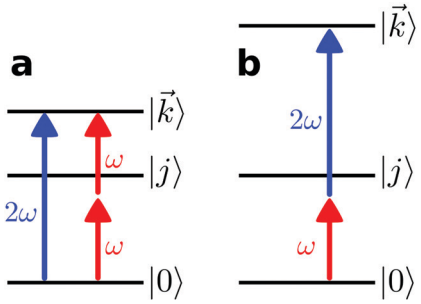

Fig. 3 (a) Simplest scheme to generate a non-zero $\tilde{b}_{1,0}$ (dichroic non-enantiosensitive) and $\tilde{b}_{2,-2}$ (dichroic and enantiosensitive) using the field (2). (b) Simplest scheme to generate a non-zero $\tilde{b}_{3,-2}$ (enantiosensitive non-dichroic) using the field (2). $|0\rangle$ and $|j\rangle$ are bound states and $|\vec{k}\rangle$ is a continuum state.

not enantiosensitive. The expression for $f_{1,0}$ reads as

$$f_{1,0} \equiv \left(\hat{z}\cdot\vec{E}^{*}_{2\omega}\right)\left(\vec{E}_{\omega}\cdot\vec{E}_{\omega}\right) = E_{2\omega}E_{\omega}^{2}e^{i\phi}, \quad (4)$$

where $\vec{E}_{2\omega} \equiv E_{2\omega}e^{-i\phi}\hat{z}$, $\vec{E}_{\omega} \equiv E_{\omega}\hat{x}$. Eqn (4) shows that the setup rotational invariant $f_{1,0}$ is a scalar involving the field vectors $\vec{E}_{2\omega}$ and $\vec{E}_{\omega}$, and the $\hat{z}$ axis. As discussed in Section 3, the axis vector $\hat{z}$ is defined by the detector needed to measure $\tilde{b}_{1,0}$. From eqn (4) it is evident that $f_{1,0}$ changes sign when ϕ is shifted by π, and therefore $\tilde{b}_{1,0}$ is dichroic.

Similarly, the interference between the two pathways in Fig. 3a gives rise to a non-zero orientation-averaged $\tilde{b}_{2,-2}$ given by (see Appendix C)

$$\tilde{b}_{2,-2} = A^{(1)*}A^{(2)}g_{2,-2}f_{2,-2} + \text{c.c.}, \quad (5)$$

where the molecular rotational invariant $g_{2,-2}$ is a (complex-valued) pseudoscalar and therefore $\tilde{b}_{2,-2}$ is enantiosensitive. The setup rotational invariant, given by

$$f_{2,-2} \equiv \left[\hat{x}\cdot\left(\hat{y}\times\vec{E}^{*}_{2\omega}\right)\right]\left(\vec{E}_{\omega}\cdot\vec{E}_{\omega}\right) = E_{2\omega}E_{\omega}^{2}e^{i\phi}, \quad (6)$$

is also a pseudoscalar and it involves the $\hat{x}$ and $\hat{y}$ axes, which are defined by the detector needed to measure $\tilde{b}_{2,-2}$ (see Section 3). Just like $g_{2,-2}$ is a pseudoscalar that distinguishes between molecules with opposite handedness, $f_{2,-2}$ is a pseudoscalar that distinguishes between chiral setups of opposite handedness. Note that the detector for $\tilde{b}_{2,-2}$ does not directly tell apart a positive x from a negative x, or a positive y from a negative y. It only tells apart positive correlations of x and y from negative correlations of x and y. This is consistent with the invariance of $f_{2,-2}$ with respect to a simultaneous inversion of $\hat{x}$ and $\hat{y}$. Furthermore, eqn (6) shows that $f_{2,-2}$ changes sign when ϕ is shifted by π, and therefore $\tilde{b}_{2,-2}$ is dichroic. We remark, that although the right hand side of eqn (4) and (6) look exactly the same after performing the vector operations, $f_{1,0}$ and $f_{2,-2}$ emerge from different setup rotational invariants of a different physical nature: one is a scalar involving only the $\hat{z}$ axis, and the other is a pseudoscalar involving correlation between the $\hat{x}$ and $\hat{y}$ axes.

We consider now the simplest process leading to the enantiosensitive but not dichroic term $\tilde{b}_{3,-2}$, *i.e.* we consider the absorption of one ω photon and one 2ω photon, resonantly enhanced through a bound state as shown in Fig. 3b. In this case we get (see Appendix D)

$$\tilde{b}_{3,-2}(k) = |A^{(2)}|^{2}g_{3,-2}f_{3,-2}, \quad (7)$$

where the rotational invariant $g_{3,-2}$ is a (real-valued) pseudoscalar, which makes $\tilde{b}_{3,-2}$ enantiosensitive. The setup rotational invariant $f_{3,-2}$ is given by

$$f_{3,-2} \equiv [\hat{x}\cdot(\hat{y}\times\hat{z})]\left(\vec{E}^{\mathrm{L}*}_{2\omega}\cdot\vec{E}_{2\omega}\right)\left(\vec{E}^{\mathrm{L}*}_{\omega}\cdot\vec{E}_{\omega}\right) = E_{\omega}^{2}E_{2\omega}^{2}. \quad (8)$$

$f_{3,-2}$ is also a pseudoscalar, however it does not record ϕ and $\tilde{b}_{3,-2}$ is therefore not dichroic. The robustness of $f_{3,-2}$ against changes of ϕ means that recording $\tilde{b}_{3,-2}$ allows distinguishing opposite enantiomers in the absence of stabilization of the ω–2ω phase shift ϕ.

Eqn (3)–(8) confirm our expectations based on general symmetry arguments according to which $\tilde{b}_{1,0}$ is dichroic and non-enantiosensitive, $\tilde{b}_{2,-2}$ is dichroic and enantiosensitive, and $\tilde{b}_{3,-2}$ is enantiosensitive and non-dichroic. In addition, these equations show that $\tilde{b}_{1,0}$, $\tilde{b}_{2,-2}$, and $\tilde{b}_{3,-2}$ are in general not zero for the specific processes considered here. This is important because although a given $\tilde{b}_{l,m}$ may be symmetry allowed according to the general symmetry analysis above, further "hidden" symmetries¶ involved in a specific process

¶ Symmetries not immediately apparent from the geometric symmetries of the system.[37]

may forbid it. For example, although the geometry of a monochromatic elliptical field allows for a non-zero $\tilde{b}_{3,-2}$, the presence of the triple product in eqn (8) means that opposite photon orderings contribute to $\tilde{b}_{3,-2}$ with opposite signs (see Appendix E). Such photon orderings are degenerate in the monochromatic case and thus the two contributions cancel each other out (see Appendix F). However, it must be kept in mind that the hidden symmetry preventing a non-zero $\tilde{b}_{3,-2}$ for elliptical fields is specific to the 2-photon process we investigated here, so it may be broken in higher order processes or in the strong field regime. That is, photoionization induced by elliptically polarized strong fields may indeed yield a non-zero enantiosensitive and non-dichroic $\tilde{b}_{3,-2}$ coefficient. This would be analogous to how $\tilde{b}_{2,-2}$ is symmetry-forbidden in the elliptical one-photon case[23] but it is symmetry allowed in the elliptical strong-field case.[38]

5 Conclusions

We discussed how tensorial observables offer new opportunities for constructing chiral setups able to distinguish between opposite enantiomers in isotropic samples without relying on the chirality of light. As a concrete example we considered the interaction of an ω–2ω cross polarized field with isotropic samples and we found selection rules for l and m that specify if a multipole coefficient $\tilde{b}_{l,m}$ is symmetry allowed, if it is dichroic (sensitive to changes of π in the ω–2ω relative phase), and if it is enantiosensitive. These $\tilde{b}_{l,m}$ coefficients are relevant in the description of photoelectron angular distributions and in the description of induced multipoles of bound charge distributions (discussed in ref. 27). We found that the enantiosensitivity and the dichroism of a $\tilde{b}_{l,m}$ coefficient are in general independent of each other. That is, in addition to the usual types of $\tilde{b}_{l,m}$ coefficients in isotropic samples, namely: (i) non-dichroic and non-enantiosensitive, (ii) dichroic and enantiosensitive, and (iii) dichroic and non-enantiosensitive, we found the more exotic possibility of (iv) enantiosensitive and non-dichroic $\tilde{b}_{l,m}$ coefficients.

We derived analytic expressions for the lowest rank $\tilde{b}_{l,m}$ coefficients in photoelectron angular distributions corresponding to types (ii)–(iv) for the case of one- *vs.* two-photon absorption and for the case of $\omega + 2\omega$ absorption. Unlike type (ii) coefficients, type (iv) coefficients allow enantiomeric discrimination in the absence of stabilization of the ω–2ω relative phase and remain to be numerically calculated and experimentally observed. Such verification is within reach with current theoretical[39] and experimental[40,41] capabilities which provide access to the full photoelectron momentum distribution. Imaging of the type (iv) coefficient $\tilde{b}_{3,-2}$ discussed here with a velocity map imaging detector as *e.g.* in ref. 26 is complicated by two facts: (a) the lack of cylindrical symmetry prevents Abel inversion and (b) projection of the $\tilde{Y}_{3,-2}$ contribution to the momentum distribution on the xy (or yz) plane cancels exactly (see Fig. 1c). However, re-orientation of the detector so as to project the momentum distribution on *e.g.* the $x = z$ plane, as shown in Fig. 4, should facilitate imaging the non-zero $\tilde{b}_{3,-2}$ coefficient. Experimentally, one can keep the detector fixed and instead rotate the polarizations of the fields. That is, measurement of the $\tilde{b}_{3,-2}$ coefficient only requires rotating ω and 2ω by 45° around their propagation axis in ref. 24 and 26.

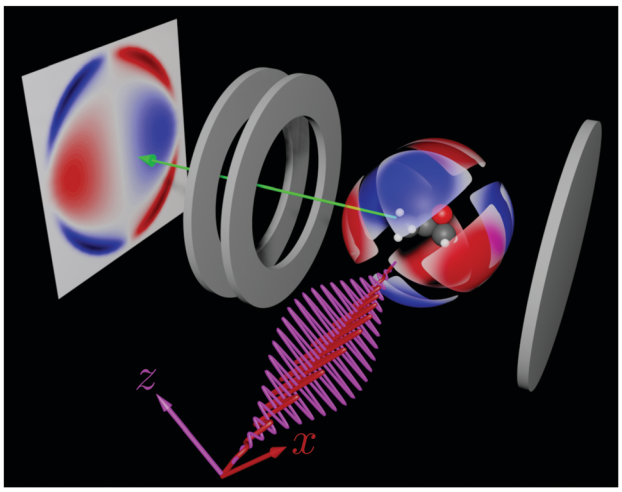

Fig. 4 Proposed velocity map imaging setup to measure the coefficient $\tilde{b}_{3,-2}$: ω (red wave) and 2ω (violet wave) are polarized along x and z, respectively. The detector projects the distribution on the $x = z$ plane. Only the contribution of $\tilde{b}_{3,-2}$ to the photoelectron angular distribution is shown. In red/blue regions there is an excess/deficit of photoelectrons.

Finally, it is also possible to obtain the type (iv) coefficient $\tilde{b}_{3,-2}$ using monochromatic light with elliptical polarization. However, a "hidden" symmetry associated to the degeneracy in photon orderings in the monochromatic case prevents this coefficient in the case of a two-photon process. The possibility of this hidden symmetry to be violated for higher-order or strong-field processes, or in a more refined description of photoionization remains to be investigated.

Conflicts of interest

There are no conflicts to declare.

Appendix

A Selection rules for an alternative orientation of the field

In Section 4 we chose the orientation of the field so as to simplify as much as possible the selection rules for the $\tilde{b}_{l,m}$ coefficients. Here, for the sake of comparison, we consider the alternative orientation‖ used in ref. 24–26, namely

$$\vec{E}(t) = E_\omega \cos(\omega t)\hat{y} + E_{2\omega}\cos(2\omega t + \phi)\hat{x}. \quad (9)$$

‖ Another sensible choice, which slightly reduces the number of non-zero $\tilde{b}_{l,m}$ coefficients, is to take the ω field along the z axis in order to obtain $\tilde{b}_{2N,m} = 0$ for $m \neq 0$ in the signal corresponding to N-photon absorption of the ω field.

Table 4 Same as Table 1 for the orientation (9)

$\tilde{b}_{l,m}$	(l,m) condition
Non-zero $2n\omega$	(Even $l-m$ and $m \geq 0$) or (odd $l-m$ and $m < 0$)
Non-zero $(2n+1)\omega$	(Odd $l-m$ and $m \geq 0$) or (even $l-m$ and $m < 0$)
Enantiosensitive	Odd $l-m$
Dichroic	[(Odd l) and ($m \geq 0$)] or [(even l) and $m < 0$]

Tables 4–6 show the analogues of Tables 1–3 for the orientation in eqn (9). In this case, we see that *e.g.* $\tilde{b}_{1,1}$, $\tilde{b}_{2,-1}$, and $\tilde{b}_{3,-2}$ are dichroic non-enantiosensitive, enantiosensitive and dichroic, and enantiosensitive non-dichroic, respectively. These are just the correspondingly rotated versions of the coefficients in Section 4. Note that $\tilde{b}_{2,-1} \propto \mathrm{Im}\{b_{2,1}\}$ is indeed the coefficient discussed in ref. 25.

B Derivation of $\tilde{b}_{1,0}$ in eqn (3)

The process depicted in Fig. 3a yields a $\tilde{b}_{1,0}$ coefficient given by[23]

$$\begin{aligned}\tilde{b}_{1,0} &= \int \mathrm{d}\Omega_k^{\mathrm{M}} \int \mathrm{d}\rho\, \tilde{Y}_1^0(\hat{k}^{\mathrm{L}}) W^{\mathrm{M}}(\vec{k}^{\mathrm{M}}, \rho) \\ &= \sqrt{\frac{3}{4\pi}} A^{(1)*} A^{(2)} \int \mathrm{d}\Omega_k^{\mathrm{M}} \int \mathrm{d}\rho \left(\hat{k}^{\mathrm{L}} \cdot \hat{z}^{\mathrm{L}}\right) \\ &\quad \times \left(\vec{d}^{\mathrm{L}}_{\vec{k}^{\mathrm{M}},0} \cdot \vec{E}^{\mathrm{L}}_{2\omega}\right)^* \left(\vec{d}^{\mathrm{L}}_{\vec{k}^{\mathrm{M}},j} \cdot \vec{E}^{\mathrm{L}}_{\omega}\right) \left(\vec{d}^{\mathrm{L}}_{j,0} \cdot \vec{E}^{\mathrm{L}}_{\omega}\right) + \text{c.c.},\end{aligned} \tag{10}$$

where c.c. denotes the complex conjugate, L and M indicate vectors and functions in the laboratory (L) and molecular (M) frames, $\vec{k}$ is the photoelectron momentum, $\hat{k} \equiv \vec{k}/k$, $\rho \equiv \alpha\beta\gamma$ is the molecular orientation specified by the Euler angles $\alpha\beta\gamma$, $\int \mathrm{d}\rho \equiv \int_0^{2\pi} \mathrm{d}\alpha \int_0^{\pi} \mathrm{d}\beta \int_0^{2\pi} \mathrm{d}\gamma \sin\beta/8\pi^2$ is the normalized integral over all molecular orientations, $\int \mathrm{d}\Omega_k^{\mathrm{M}}$ is the integral over all photoelectron directions $\hat{k}^{\mathrm{M}}$, $W^{\mathrm{M}}(\vec{k}^{\mathrm{M}}, \rho) \equiv |a_{\vec{k}^{\mathrm{M}}}(\rho)|^2$ is the photoelectron angular distribution in the molecular frame for a particular orientation ρ. $a_{\vec{k}^{\mathrm{M}}}(\rho) = A^{(1)}(\vec{d}^{\mathrm{L}}_{\vec{k}^{\mathrm{M}},0} \cdot \vec{E}^{\mathrm{L}}_{2\omega}) + A^{(2)}(\vec{d}^{\mathrm{L}}_{\vec{k}^{\mathrm{M}},j} \cdot \vec{E}^{\mathrm{L}}_{\omega})(\vec{d}^{\mathrm{L}}_{j,0} \cdot \vec{E}^{\mathrm{L}}_{\omega})$ is the probability amplitude of the state $|\vec{k}^{\mathrm{M}}\rangle$, $A^{(1)}$ and $A^{(2)}$ are complex-valued constants depending on detunings and pulse envelopes, $\vec{d}_{i,j} \equiv \langle i|\vec{d}|j\rangle$ is the dipole transition matrix element between states $|i\rangle$ and $|j\rangle$, $|\vec{k}\rangle$ is the scattering state describing an outgoing plane wave with photoelectron momentum $\vec{k}$, and $\vec{E}_{\omega} = E_{\omega}\hat{x}$ and $\vec{E}_{2\omega} = E_{2\omega} e^{-i\phi}\hat{z}$ are the Fourier amplitudes of the field (2) at frequencies ω and 2ω, respectively. The vectors $\hat{k}^{\mathrm{L}}$ and $\vec{d}^{\mathrm{L}}_{i,j}$, depend on the molecular orientation ρ according to $\vec{v}^{\mathrm{L}} = S(\rho)\vec{v}^{\mathrm{M}}$, where $S(\rho)$ is the rotation matrix taking vectors from the molecular frame to the laboratory frame. Note that only the interference between the two pathways in Fig. 3 contributes to $\tilde{b}_{1,0}$ (see Section 4).

The integral over orientations yields[23,42]

$$\int \mathrm{d}\rho \left(\hat{k}^{\mathrm{L}} \cdot \hat{z}^{\mathrm{L}}\right) \left(\vec{d}^{\mathrm{L}}_{\vec{k}^{\mathrm{M}},0} \cdot \vec{E}^{\mathrm{L}}_{2\omega}\right)^* \left(\vec{d}^{\mathrm{L}}_{\vec{k}^{\mathrm{M}},j} \cdot \vec{E}^{\mathrm{L}}_{\omega}\right) \left(\vec{d}^{\mathrm{L}}_{j,0} \cdot \vec{E}^{\mathrm{L}}_{\omega}\right) = \vec{g}^{(4)} \cdot M^{(4)} \vec{f}^{(4)}, \tag{11}$$

where $\vec{g}^{(4)}$ and $\vec{f}^{(4)}$ are vectors of molecular and setup rotational invariants, respectively,

$$\vec{g}^{(4)} = \begin{bmatrix} \left(\hat{k}^{\mathrm{M}} \cdot \vec{d}^{\mathrm{M}*}_{\vec{k}^{\mathrm{M}},0}\right)\left(\vec{d}^{\mathrm{M}}_{\vec{k}^{\mathrm{M}},j} \cdot \vec{d}^{\mathrm{M}}_{j,0}\right) \\ \left(\hat{k}^{\mathrm{M}} \cdot \vec{d}^{\mathrm{M}}_{\vec{k}^{\mathrm{M}},j}\right)\left(\vec{d}^{\mathrm{M}*}_{\vec{k}^{\mathrm{M}},0} \cdot \vec{d}^{\mathrm{M}}_{j,0}\right) \\ \left(\hat{k}^{\mathrm{M}} \cdot \vec{d}^{\mathrm{M}}_{j,0}\right)\left(\vec{d}^{\mathrm{M}*}_{\vec{k}^{\mathrm{M}},0} \cdot \vec{d}^{\mathrm{M}}_{\vec{k}^{\mathrm{M}},j}\right) \end{bmatrix}, \tag{12}$$

$$M^{(4)} = \frac{1}{30}\begin{bmatrix} 4 & -1 & -1 \\ -1 & 4 & -1 \\ -1 & -1 & 4 \end{bmatrix}, \tag{13}$$

$$\begin{aligned}\vec{f}^{(4)} &= \begin{bmatrix} \left(\hat{z}^{\mathrm{L}} \cdot \vec{E}^{\mathrm{L}*}_{2\omega}\right)\left(\vec{E}^{\mathrm{L}}_{\omega} \cdot \vec{E}^{\mathrm{L}}_{\omega}\right) \\ \left(\hat{z}^{\mathrm{L}} \cdot \vec{E}^{\mathrm{L}}_{\omega}\right)\left(\vec{E}^{\mathrm{L}*}_{2\omega} \cdot \vec{E}^{\mathrm{L}}_{\omega}\right) \\ \left(\hat{z}^{\mathrm{L}} \cdot \vec{E}^{\mathrm{L}}_{\omega}\right)\left(\vec{E}^{\mathrm{L}*}_{2\omega} \cdot \vec{E}^{\mathrm{L}}_{\omega}\right) \end{bmatrix} \\ &= \begin{bmatrix} \left(\hat{z}^{\mathrm{L}} \cdot \vec{E}^{\mathrm{L}*}_{2\omega}\right)\left(\vec{E}^{\mathrm{L}}_{\omega} \cdot \vec{E}^{\mathrm{L}}_{\omega}\right) \\ 0 \\ 0 \end{bmatrix}.\end{aligned} \tag{14}$$

Replacing eqn (11)–(14) in eqn (10) we obtain eqn (3), where $f_{1,0}$ is given by eqn (4) and $g_{1,0}$ is given by

$$\begin{aligned}g_{1,0} &\equiv \frac{1}{30}\sqrt{\frac{3}{4\pi}} \int \mathrm{d}\Omega_k^{\mathrm{M}} \Big[4\left(\hat{k}^{\mathrm{M}} \cdot \vec{d}^{\mathrm{M}*}_{\vec{k}^{\mathrm{M}},0}\right)\left(\vec{d}^{\mathrm{M}}_{\vec{k}^{\mathrm{M}},j} \cdot \vec{d}^{\mathrm{M}}_{j,0}\right) \\ &\quad - \left(\hat{k}^{\mathrm{M}} \cdot \vec{d}^{\mathrm{M}}_{\vec{k}^{\mathrm{M}},j}\right)\left(\vec{d}^{\mathrm{M}*}_{\vec{k}^{\mathrm{M}},0} \cdot \vec{d}^{\mathrm{M}}_{j,0}\right) - \left(\hat{k}^{\mathrm{M}} \cdot \vec{d}^{\mathrm{M}}_{j,0}\right)\left(\vec{d}^{\mathrm{M}*}_{\vec{k}^{\mathrm{M}},0} \cdot \vec{d}^{\mathrm{M}}_{\vec{k}^{\mathrm{M}},j}\right)\Big].\end{aligned} \tag{15}$$

We remark that eqn (3), (4) and (15) are not valid for arbitrary polarizations of $\vec{E}_{\omega}$ and $\vec{E}_{2\omega}$. We have kept the vectorial form of the rotational invariant in eqn (4) to emphasize the scalar *vs.* pseudoscalar character (see discussion in Section 4.1). As can be seen from eqn (14), to derive eqn (3), (4) and (15) we explicitly used $\vec{E}^{\mathrm{L}}_{2\omega} \| \hat{z}^{\mathrm{L}}$ and $\vec{E}^{\mathrm{L}}_{\omega} \| \hat{x}^{\mathrm{L}}$.

C Derivation of $\tilde{b}_{2,-2}$ in eqn (5)

Similarly, for the $\tilde{b}_{2,-2}$ coefficient we have[23]

$$\begin{aligned}\tilde{b}_{2,-2} &= \int \mathrm{d}\Omega_k^{\mathrm{M}} \int \mathrm{d}\rho\, \tilde{Y}_2^{-2}(\vec{k}^{\mathrm{L}}) W^{\mathrm{M}}(\vec{k}^{\mathrm{M}}, \rho) \\ &= \frac{1}{2}\sqrt{\frac{15}{\pi}} A^{(1)*} A^{(2)} \int \mathrm{d}\Omega_k^{\mathrm{M}} \int \mathrm{d}\rho \left(\hat{k}^{\mathrm{L}} \cdot \hat{x}^{\mathrm{L}}\right)\left(\hat{k}^{\mathrm{L}} \cdot \hat{y}^{\mathrm{L}}\right) \\ &\quad \times \left(\vec{d}^{\mathrm{L}}_{\vec{k}^{\mathrm{M}},0} \cdot \vec{E}^{\mathrm{L}}_{2\omega}\right)^* \left(\vec{d}^{\mathrm{L}}_{\vec{k}^{\mathrm{M}},j} \cdot \vec{E}^{\mathrm{L}}_{\omega}\right) \left(\vec{d}^{\mathrm{L}}_{j,0} \cdot \vec{E}^{\mathrm{L}}_{\omega}\right) + \text{c.c.}\end{aligned} \tag{16}$$

The integral over orientations can be performed analogously to what we did for $\tilde{b}_{1,0}$.[42] Making explicit use of $\vec{E}^{\mathrm{L}}_{2\omega} \| \hat{z}^{\mathrm{L}}$ and $\vec{E}^{\mathrm{L}}_{\omega} \| \hat{x}^{\mathrm{L}}$

Table 5 Same as Table 2 for the orientation of the field used in eqn (9)

$\tilde{b}_{l,m}$	(l,m) condition at $2n\omega$	(l,m) condition at $(2n+1)\omega$
Enantiosensitive and dichroic	(Even l) and (odd $m<0$)	(Odd l) and (even $m\geq 0$)
Enantiosensitive non-dichroic	(Odd l) and (even $m<0$)	(Even l) and (odd $m\geq 0$)
Dichroic non-enantiosensitive	(Odd l) and (odd $m\geq 0$)	(Even l) and (even $m<0$)

Table 6 Same as Table 3 for the orientation of the field used in eqn (9)

Symmetry-allowed	$\tilde{b}_{0,0}$	$\tilde{b}_{1,1}$	$\tilde{b}_{2,-1}$	$\tilde{b}_{2,0}$	$\tilde{b}_{2,2}$	$\tilde{b}_{3,-2}$	$\tilde{b}_{3,1}$	$\tilde{b}_{3,3}$	$\tilde{b}_{4,-3}$	$\tilde{b}_{4,-1}$	$\tilde{b}_{4,0}$	$\tilde{b}_{4,2}$	$\tilde{b}_{4,4}$
Enantiosensitive	N	N	Y	N	N	Y	N	N	Y	Y	N	N	N
Dichroic	N	Y	Y	N	N	N	Y	Y	Y	Y	N	N	N

yields eqn (5), with $f_{2,-2}$ given by eqn (6) and $g_{2,-2}$ given by

$$g_{2,-2} \equiv \frac{1}{4\sqrt{15\pi}}\int d\Omega_k^M \Big\{ \Big[\hat{k}^M \cdot \Big(\vec{d}^{M*}_{\hat{k}^M,0} \times \vec{d}^{M}_{\hat{k}^M,j}\Big)\Big]\Big(\hat{k}^M \cdot \vec{d}^{M}_{j,0}\Big) + \Big[\hat{k}^M \cdot \Big(\vec{d}^{M*}_{\hat{k}^M,0} \times \vec{d}^{M}_{j,0}\Big)\Big]\Big(\hat{k}^M \cdot \vec{d}^{M}_{\hat{k}^M,j}\Big)\Big\}. \quad (17)$$

We point out that when dealing with integrals over orientations involving five or more scalar products, the number of rotational invariants that can be formed is such that they are no longer linearly independent from each other.[42] As a result it is possible to write the result of the integral in several different ways that, although perfectly equivalent, are not evidently related to each other at first sight. For example, by changing the order of the scalar products in such a way that $(\vec{d}^{L}_{\hat{k},j} \cdot \vec{E}^{L}_{\omega})$ exchanges its position with $(\hat{k}^L \cdot \hat{x}^L)$ in eqn (15) one obtains

$$\tilde{b}_{2,-2} = A^{(1)*}A^{(2)}g'_{2,-2}f'_{2,-2} + \text{c.c.}, \quad (18)$$

where

$$g'_{2,-2} \equiv \frac{1}{4\sqrt{15\pi}}\int d\Omega_k^M \Big\{ 2\Big[\vec{d}^{M}_{\hat{k}^M,j} \cdot \Big(\hat{k}^M \times \vec{d}^{M*}_{\hat{k}^M,0}\Big)\Big]\Big(\hat{k}^M \cdot \vec{d}^{M}_{j,0}\Big) - \Big[\vec{d}^{M}_{\hat{k}^M,j} \cdot \Big(\hat{k}^M \times \vec{d}^{M}_{j,0}\Big)\Big]\Big(\vec{d}^{M*}_{\hat{k}^M,0} \cdot \hat{k}^M\Big) + \Big[\vec{d}^{M}_{\hat{k}^M,j} \cdot \Big(\vec{d}^{M*}_{\hat{k}^M,0} \times \vec{d}^{M}_{j,0}\Big)\Big]\Big(\hat{k}^M \cdot \hat{k}^M\Big)\Big\}, \quad (19)$$

$$f'_{2,-2} \equiv \Big[\vec{E}^{L}_{\omega} \cdot \Big(\hat{y}^L \times \vec{E}^{L*}_{2\omega}\Big)\Big]\Big(\hat{x}^L \cdot \vec{E}^{L}_{\omega}\Big), \quad (20)$$

and again we assumed that $\vec{E}^{L}_{2\omega} \| \hat{z}^L$ and $\vec{E}^{L}_{\omega} \| \hat{x}^L$. Writing the explicit expressions $\vec{E}_{\omega} = E_{\omega}\hat{x}$ and $\vec{E}^{*}_{2\omega} = E_{2\omega}e^{i\phi}\hat{z}$ one can show that $f'_{2,-2} = f_{2,-2}$. And using standard vectorial algebra relations one can show that $g'_{2,-2} = g_{2,2}$. The latter equality reflects the fact that, for four arbitrary vectors $\vec{a}$, $\vec{b}$, $\vec{c}$, $\vec{d}$, the three different rotational invariants $r_1 \equiv [\vec{a}\cdot(\vec{b}\times\vec{c})](\vec{b}\cdot\vec{d})$, $r_2 \equiv [\vec{a}\cdot(\vec{b}\times\vec{d})](\vec{c}\cdot\vec{b})$, and $r_3 \equiv [\vec{a}\cdot(\vec{c}\times\vec{d})](\vec{b}\cdot\vec{b})$ can be written as a linear combination of the *two* rotational invariants r_1 and $r_4 \equiv [\vec{b}\cdot(\vec{c}\times\vec{d})](\vec{b}\cdot\vec{a})$. Care must therefore be taken when looking for interpretations that depend on the particular ordering of the vectors appearing in the rotational invariants.

D Derivation of $\tilde{b}_{3,-2}$ for $\omega + 2\omega$ [eqn (7)]

The process depicted in Fig. 3b yields a $\tilde{b}_{3,-2}$ coefficient given by[23]

$$\tilde{b}_{3,-2}(k) = \int d\Omega_k^M \int d\rho\, \tilde{Y}_3^{-2}(\hat{k}^L) W^M(\vec{k}^M, \rho) = |A^{(2)}|^2 \frac{1}{2}\sqrt{\frac{105}{\pi}}\int d\Omega_k^M \int d\rho \Big(\hat{k}^L \cdot \hat{x}^L\Big)\Big(\hat{k}^L \cdot \hat{y}^L\Big)\Big(\hat{k}^L \cdot \hat{z}^L\Big) \times \Big|\vec{d}^{L}_{\hat{k}^M,j} \cdot \vec{E}^{L}_{2\omega}\Big|^2 \Big|\vec{d}^{L}_{j,0} \cdot \vec{E}^{L}_{\omega}\Big|^2. \quad (21)$$

The integral over orientations can be performed analogously to what we did for $\tilde{b}_{1,0}$.[42] Making explicit use of $\vec{E}^{L}_{2\omega} \| \hat{z}^L$ and $\vec{E}^{L}_{\omega} \| \hat{x}^L$ yields eqn (7), with $f_{3,-2}$ given by eqn (8) and $g_{3,-2}$ given by**

$$g_{3,-2} \equiv \frac{1}{8\sqrt{105\pi}}\int d\Omega_k^M \Big[\hat{k}^M \cdot \Big(\vec{d}^{M}_{j,0} \times \vec{d}^{M*}_{\hat{k}^M,j}\Big)\Big] \times \Big[\Big(\vec{d}^{M}_{\hat{k}^M,j} \cdot \vec{d}^{M}_{j,0}\Big) - 5\Big(\hat{k}^M \cdot \vec{d}^{M}_{\hat{k}^M,j}\Big)\Big(\hat{k}^M \cdot \vec{d}^{M}_{j,0}\Big)\Big] + \text{c.c.}, \quad (22)$$

E Derivation of $\tilde{b}_{3,-2}$ for $2\omega + \omega$: symmetry in photon ordering

First we rewrite the integral over orientations in eqn (21) as

$$I_{\omega,2\omega}\big(\hat{x}^L, \hat{y}^L, \hat{z}^L\big) = |E_{\omega}|^2|E_{2\omega}|^2 \int d\rho \Big(\hat{k}^L \cdot \hat{x}^L\Big)\Big(\hat{k}^L \cdot \hat{y}^L\Big)\Big(\hat{k}^L \cdot \hat{z}^L\Big) \times \Big|\Big(\vec{d}^{L}_{\hat{k}^M,j} \cdot \hat{z}^L\Big)\Big(\vec{d}^{L}_{j,0} \cdot \hat{x}^L\Big)\Big|^2. \quad (23)$$

** This is considerably simplified by ordering the scalar products in the orientation integral as $(\hat{k}^L \cdot \hat{x}^L)(\hat{k}^L \cdot \hat{z}^L)(\vec{d}^{L*}_{j,0} \cdot \vec{E}^{L*}_{\omega})(\hat{k}^L \cdot \hat{y}^L)(\vec{d}^{L*}_{\hat{k}^M,j} \cdot \vec{E}^{L*}_{2\omega})(\vec{d}^{L}_{\hat{k}^M,j} \cdot \vec{E}^{L}_{2\omega})(\vec{d}^{L}_{j,0} \cdot \vec{E}^{L}_{\omega})$ and using Table III in ref. 42.

For the opposite photon ordering we have

$$\begin{aligned} I_{2\omega,\omega}(\hat{x}^{\mathrm{L}},\hat{y}^{\mathrm{L}},\hat{z}^{\mathrm{L}}) &= |E_\omega|^2|E_{2\omega}|^2\int \mathrm{d}\rho\left(\hat{k}^{\mathrm{L}}\cdot\hat{z}^{\mathrm{L}}\right)\left(\hat{k}^{\mathrm{L}}\cdot\hat{y}^{\mathrm{L}}\right)\left(\hat{k}^{\mathrm{L}}\cdot\hat{x}^{\mathrm{L}}\right)\\ &\quad\times\left|\left(\vec{d}^{\mathrm{L}}_{\bar{k}^{\mathrm{M}},j}\cdot\hat{x}^{\mathrm{L}}\right)\left(\vec{d}^{\mathrm{L}}_{j,0}\cdot\hat{z}^{\mathrm{L}}\right)\right|^2\\ &= I_{\omega,2\omega}(\hat{z}^{\mathrm{L}},\hat{y}^{\mathrm{L}},\hat{x}^{\mathrm{L}}), \end{aligned} \tag{24}$$

that is, reversing the photon ordering is equivalent to the exchanging $\hat{x}^{\mathrm{L}}$ and $\hat{z}^{\mathrm{L}}$ in eqn (23). On the other hand, from the triple product in eqn (8) it follows that

$$I_{\omega,2\omega}(\hat{z}^{\mathrm{L}},\hat{y}^{\mathrm{L}},\hat{x}^{\mathrm{L}}) = -I_{\omega,2\omega}(\hat{x}^{\mathrm{L}},\hat{y}^{\mathrm{L}},\hat{z}^{\mathrm{L}}) \tag{25}$$

and thus

$$I_{2\omega,\omega}(\hat{x}^{\mathrm{L}},\hat{y}^{\mathrm{L}},\hat{z}^{\mathrm{L}}) = -I_{\omega,2\omega}(\hat{x}^{\mathrm{L}},\hat{y}^{\mathrm{L}},\hat{z}^{\mathrm{L}}). \tag{26}$$

This means that the expression for $\tilde{b}_{3,-2}$ in the photon ordering $2\omega+\omega$ is exactly the same as for the photon ordering $\omega+2\omega$ up to a minus sign. However, since for a fixed molecular spectrum the coupling coefficient $A^{(2)}$ strongly depends on detunings (and therefore photon ordering), if one of the photon orderings is resonant it will dominate. Furthermore, in practice each photon ordering might be resonant with different transitions, and one should therefore use different transition dipole matrix elements for each ordering.

Since the derivation we just presented is actually independent of the frequencies, we have that

$$I_{\omega_1,\omega_2} = -I_{\omega_2,\omega_1}, \tag{27}$$

provided ω_1 and ω_2 have linear polarizations perpendicular to each other. We can therefore conclude that $\tilde{b}_{3,-2}\to 0$ as $\omega_1\to\omega_2$. Note that this is analogous to the corresponding result for the polarization in sum-frequency generation.[43]

F Vanishing of $\tilde{b}_{3,-2}$ for elliptical light

Using relation (27) it is simple to establish why, although a monochromatic elliptical field has a geometry that allows for a non-zero $\tilde{b}_{3,-2}$ in an $\omega+2\omega$ process, the "hidden" symmetry in eqn (27) forces it to vanish. To see this, note that for an elliptical field we have

$$\vec{E}(t) = \vec{E}_\omega \mathrm{e}^{-i\omega t} + \text{c.c.}, \tag{28}$$

with $\vec{E}_\omega = E_\omega\hat{x} + iE_y\hat{y}$ and therefore [*cf.* eqn (21)]

$$\begin{aligned} &W^{\mathrm{M}}(\bar{k}^{\mathrm{M}},\rho)\\ &=\left|A^{(2)}\right|^2\left|\vec{d}^{\mathrm{L}}_{\bar{k}^{\mathrm{M}},j}\cdot\vec{E}^{\mathrm{L}}_\omega\right|^2\left|\vec{d}^{\mathrm{L}}_{j,0}\cdot\vec{E}^{\mathrm{L}}_\omega\right|^2\\ &=\left|A^{(2)}\right|^2\Big\{\left|\vec{d}^{\mathrm{L}}_{\bar{k}^{\mathrm{M}},j}\cdot E_x\hat{x}^{\mathrm{L}}\right|^2\left|\vec{d}^{\mathrm{L}}_{j,0}\cdot E_x\hat{x}^{\mathrm{L}}\right|^2+\left|\vec{d}^{\mathrm{L}}_{\bar{k}^{\mathrm{M}},j}\cdot E_y\hat{y}^{\mathrm{L}}\right|^2\left|\vec{d}^{\mathrm{L}}_{j,0}\cdot E_y\hat{y}^{\mathrm{L}}\right|^2\\ &\quad+\left|\vec{d}^{\mathrm{L}}_{\bar{k}^{\mathrm{M}},j}\cdot E_x\hat{x}^{\mathrm{L}}\right|^2\left|\vec{d}^{\mathrm{L}}_{j,0}\cdot E_y\hat{y}^{\mathrm{L}}\right|^2+\left|\vec{d}^{\mathrm{L}}_{\bar{k}^{\mathrm{M}},j}\cdot E_y\hat{y}^{\mathrm{L}}\right|^2\left|\vec{d}^{\mathrm{L}}_{j,0}\cdot E_x\hat{x}^{\mathrm{L}}\right|^2\\ &\quad+\left(i\vec{d}^{\mathrm{L}*}_{\bar{k}^{\mathrm{M}},j}\times i\vec{d}^{\mathrm{L}}_{\bar{k}^{\mathrm{M}},j}\right)\cdot\left(E_x\hat{x}^{\mathrm{L}}\times E_y\hat{y}^{\mathrm{L}}\right)\left(\left|\vec{d}^{\mathrm{L}}_{\bar{k}^{\mathrm{M}},j}\cdot E_x\hat{x}^{\mathrm{L}}\right|^2+\left|\vec{d}^{\mathrm{L}}_{j,0}\cdot E_y\hat{y}^{\mathrm{L}}\right|^2\right)\Big\}, \end{aligned} \tag{29}$$

that is, we can decompose the process into six pathways. The first two of them involve either two x-polarized photons or two y-polarized photons and the associated geometrical symmetry prevents them from contributing to $\tilde{b}_{3,-2}$. The next two terms involve absorption of one x-polarized photon and one y-polarized photon and their lower geometrical symmetry allows for contributions to $\tilde{b}_{3,-2}$. However, since these two terms correspond to opposite photon orderings satisfying $\omega_1\to\omega_2$, the photon-ordering symmetry in eqn (27) implies that their contributions will cancel each other exactly. The remaining terms describe PECD from the state $|j\rangle$ [cf. eqn (10) in ref. 13] after excitation *via* either an x- or a y-polarized photon. These terms make a null contribution to the integral over orientations in $\tilde{b}_{3,-2}$ because all possible setup rotational invariants that can be formed either with the set $\{\hat{x}^{\mathrm{L}},\hat{y}^{\mathrm{L}},\hat{z}^{\mathrm{L}},(E_x\hat{x}^{\mathrm{L}}\times\hat{E}_y\hat{y}^{\mathrm{L}}),E_x\hat{x}^{\mathrm{L}},E_x\hat{x}^{\mathrm{L}}\}$ or with the set $\{\hat{x}^{\mathrm{L}},\hat{y}^{\mathrm{L}},\hat{z}^{\mathrm{L}},(E_x\hat{x}^{\mathrm{L}}\times\hat{E}_y\hat{y}^{\mathrm{L}}),E_y\hat{y}^{\mathrm{L}},E_y\hat{y}^{\mathrm{L}}\}$ vanish.[42]

Acknowledgements

A. F. O. and O. S. gratefully acknowledge the MEDEA Project, which has received funding from the European Union's Horizon 2020 Research and Innovation Programme under the Marie Skłodowska-Curie Grant Agreement No. 641789. A. F. O. and O. S. gratefully acknowledge support from the DFG SPP 1840 "Quantum Dynamics in Tailored Intense Fields" and DFG Grant No. SM 292/5-2. A. F. O. gratefully acknowledges grants supporting his research at ICFO: Agencia Estatal de Investigación (the R&D project CEX2019-000910-S, funded by MCIN/AEI/10.13039/501100011033, Plan Nacional FIDEUA PID2019-106901GB-I00, FPI), Fundació Privada Cellex, Fundació Mir-Puig, Generalitat de Catalunya (AGAUR Grant No. 2017 SGR 1341, CERCA program), and EU Horizon 2020 Marie Skłodowska-Curie grant agreement no. 101029393.

Notes and references

1 T. M. Lowry, *Optical Rotatory Power*, Dover Publications, New York, 1964.
2 N. Berova, P. L. Polavarapu, K. Nakanishi and R. W. Woody, *Comprehensive Chiroptical Spectroscopy*, Wiley, Hoboken, New Jersey, 2012.
3 S. Eibenberger, J. Doyle and D. Patterson, *Phys. Rev. Lett.*, 2017, **118**, 123002.
4 A. Yachmenev, J. Onvlee, E. Zak, A. Owens and J. Küpper, *Phys. Rev. Lett.*, 2019, **123**, 243202.
5 R. E. Goetz, C. P. Koch and L. Greenman, *Phys. Rev. Lett.*, 2019, **122**, 013204.
6 D. Ayuso, O. Neufeld, A. F. Ordonez, P. Decleva, G. Lerner, O. Cohen, M. Ivanov and O. Smirnova, *Nat. Photonics*, 2019, **13**, 866.
7 T. Cao and Y. Qiu, *Nanoscale*, 2018, **10**, 566–574.
8 R. Noyori, *Angew. Chem., Int. Ed.*, 2002, **41**, 2008–2022.
9 L. D. Barron, *Molecular light scattering and optical activity*, Cambridge University Press, 2nd edn, 2004.

10 H. Rhee, Y.-G. June, J.-S. Lee, K.-K. Lee, J.-H. Ha, Z. H. Kim, S.-J. Jeon and M. Cho, *Nature*, 2009, **458**, 310–313.
11 Y. Tang and A. E. Cohen, *Science*, 2011, **332**, 333–336.
12 C. Rosales-Guzmán, K. Volke-Sepulveda and J. P. Torres, *Opt. Lett.*, 2012, **37**, 3486–3488.
13 A. F. Ordonez and O. Smirnova, *Phys. Rev. A*, 2018, **98**, 063428.
14 A. F. Ordonez, PhD thesis, Technische Universität Berlin, Berlin, Germany, 2019.
15 B. Ritchie, *Phys. Rev. A: At., Mol., Opt. Phys.*, 1976, **13**, 1411.
16 N. Böwering, T. Lischke, B. Schmidtke, N. Müller, T. Khalil and U. Heinzmann, *Phys. Rev. Lett.*, 2001, **86**, 1187–1190.
17 I. Powis, *J. Chem. Phys.*, 2000, **112**, 301–310.
18 C. Lux, M. Wollenhaupt, T. Bolze, Q. Liang, J. Köhler, C. Sarpe and T. Baumert, *Angew. Chem., Int. Ed.*, 2012, **51**, 5001–5005.
19 M. H. M. Janssen and I. Powis, *Phys. Chem. Chem. Phys.*, 2013, **16**, 856–871.
20 L. Nahon, G. A. Garcia and I. Powis, *J. Electron Spectrosc. Relat. Phenom.*, 2015, **204**(Part B), 322–334.
21 V. Ulrich, S. Barth, S. Joshi, U. Hergenhahn, E. Mikajlo, C. J. Harding and I. Powis, *J. Phys. Chem. A*, 2008, **112**, 3544–3549.
22 S. Beaulieu, A. Ferré, R. Géneaux, R. Canonge, D. Descamps, B. Fabre, N. Fedorov, F. Légaré, S. Petit, T. Ruchon, V. Blanchet, Y. Mairesse and B. Pons, *New J. Phys.*, 2016, **18**, 102002.
23 A. F. Ordonez and O. Smirnova, 2020, arXiv:2009.03660 [physics].
24 P. V. Demekhin, A. N. Artemyev, A. Kastner and T. Baumert, *Phys. Rev. Lett.*, 2018, **121**, 253201.
25 P. V. Demekhin, *Phys. Rev. A*, 2019, **99**, 063406.
26 S. Rozen, A. Comby, E. Bloch, S. Beauvarlet, D. Descamps, B. Fabre, S. Petit, V. Blanchet, B. Pons, N. Dudovich and Y. Mairesse, *Phys. Rev. X*, 2019, **9**, 031004.
27 A. F. Ordonez and O. Smirnova, in *Molecular Beams in Physics and Chemistry: From Otto Stern's Pioneering Exploits to Present-Day Feats*, ed. B. Friedrich and H. Schmidt-Böcking, Springer International Publishing, Cham, 2021, pp. 335–352.
28 D. Patterson, M. Schnell and J. M. Doyle, *Nature*, 2013, **497**, 475–477.
29 D. Patterson and J. M. Doyle, *Phys. Rev. Lett.*, 2013, **111**, 023008.
30 K. K. Lehmann, in *Frontiers and Advances in Molecular Spectroscopy*, ed. J. Laane, Elsevier, 2018, pp. 713–743.
31 D. M. Brink and G. R. Satchler, *Angular Momentum*, Clarendon Press, Oxford, 2nd edn, 1968.
32 O. Neufeld, D. Podolsky and O. Cohen, *Nat. Commun.*, 2019, **10**, 405.
33 Y.-Y. Yin, C. Chen, D. S. Elliott and A. V. Smith, *Phys. Rev. Lett.*, 1992, **69**, 2353–2356.
34 R. E. Goetz, C. P. Koch and L. Greenman, *J. Chem. Phys.*, 2019, **151**, 074106.
35 G. Wagnière, *Phys. Rev. A: At., Mol., Opt. Phys.*, 1989, **40**, 2437–2440.
36 G. H. Wagnière and G. L. J. A. Rikken, *Chem. Phys. Lett.*, 2011, **502**, 126–129.
37 A. Cisneros and H. V. McIntosh, *J. Math. Phys.*, 1970, **11**, 870–895.
38 M. Bashkansky, P. H. Bucksbaum and D. W. Schumacher, *Phys. Rev. Lett.*, 1988, **60**, 2458–2461.
39 A. D. Müller, E. Kutscher, A. N. Artemyev and P. V. Demekhin, *J. Chem. Phys.*, 2020, **152**, 044302.
40 M. Richter, M. Kunitski, M. Schöffler, T. Jahnke, L. P. H. Schmidt and R. Dörner, *Phys. Rev. A*, 2016, **94**, 033416.
41 K. Fehre, S. Eckart, M. Kunitski, C. Janke, D. Trabert, J. Rist, M. Weller, A. Hartung, L. P. H. Schmidt, T. Jahnke, R. Dörner and M. Schöffler, *J. Phys. Chem. A*, 2019, **123**, 6491–6495.
42 D. L. Andrews and T. Thirunamachandran, *J. Chem. Phys.*, 1977, **67**, 5026–5033.
43 J. A. Giordmaine, *Phys. Rev.*, 1965, **138**, A1599–A1606.